International Journal of Marine Science and Technology, vol. 2, no. 1, pp. 58–67, 2026 e-ISSN: 3093-3609
https://doi.org/10.65154/ijmst.44 https://i-jmst.vimaru.edu.vn

Integrated Energy-Optimal Control for Underactuated Surface Vessels via Adaptive Sliding Mode and High-Order Extended State Observer with Thrust Allocation

Quyen Nguyen Huu*, Cuong Nguyen Hung, and My Truong Cong

Abstract: This paper explores the problem of trajectory tracking control for Underactuated Surface Vessels (USVs) subject to unknown environmental disturbances and other uncertainties. The proposed controlled system consists of an Adaptive Sliding Mode Control (ASMC), an High-Order Extended State Observer (HO-ESO), and an energy-optimal Thrust Allocation (TA) algorithm between the propeller and the rudder. An HO-ESO is introduced to estimate unmeasured system states and unknown external disturbances, enhancing the control system's sustainability. Moreover, to improve the precision in trajectory tracking and mitigate the conventional sliding mode control's chattering phenomenon, an adaptive control law is designed to dynamically adjust control gains. Furthermore, unlike conventional control methods, input control signals are typically assumed to be ideal. An energy-optimal thrust allocation algorithm is developed to convert control signals from the controller into practical reference commands for the actuators. By establishing a nonlinear optimization problem, the proposed TA scheme helps to reduce the total amount of energy consumption while ensuring physical actuator constraints and maintaining satisfactory trajectory tracking performance. This paper also performs a stability analysis based on Lyapunov theory, which proves that all tracking errors in the closed-loop system are bounded and stable. Simulation studies, which are conducted in the Matlab-Simulink application, has validated the superiority of the proposed integrated controller, in terms of its tracking accuracy, disturbance rejection capability, and energy efficiency compared with existing methods.

Keywords: Adaptive sliding mode control, disturbance rejection, energy-optimal thrust allocation, high-order extended state observer, underactuated surface vessels.

1. INTRODUCTION

In marine vehicle control engineering, many types of vessels are designed with underactuated configurations [1], meaning that the number of independent actuators is smaller than the number of degrees of freedom to be controlled [4, 19]. This structural limitation, combined with vessels' nonlinear dynamic characteristics and unknown disturbances on marine environments bring about significant challenges for researchers studying Underactuated surface vessels, especially in trajectory tracking problems. These problems requires the adoption of advanced control strategies in order to ensure stability and operational reliability, particularly when operating in complex marine environments, characterized by unpredictable disturbances such as winds, waves, and currents [3, 9].

To maintain sustainability against these unknown disturbances from marine environments, the SMC has been widely adopted due to its strong invariance feature [6]. However, the high - frequency (chattering) phenomenon associated with the conventional SMC can cause mechanical wear and lead to the enormous and insufficient usage of energy. This is detrimental to long-term reliability of marine actuators [7, 8]. Recent studies show that controllers have further integrated adaptive schemes for online tuning of control parameters, achieving smoother control actions without sacrificing robustness [5, 12]. Despite these improvements, many existing ASMC controllers still treat control forces as direct inputs and often neglect active disturbance estimation as well as efficient force allocation among the available actuators [7, 11].

The HO-ESO is introduced as an effective solution for

Manuscript received January 28, 2026; received in revised form February 20, 2026; accepted February 27, 2026; available online March 30, 2026.

Quyen Nguyen Huu, Cuong Nguyen Hung, and My Truong Cong are with the Faculty of Electrical and Electronic Engineering, Vietnam Maritime University, Haiphong, Vietnam (e-mails: quyennh.ddt@vimaru.edu.vn, cuongnh.ddt@vimaru.edu.vn, and mytc.ddt@vimaru.edu.vn).
* Corresponding author.

active disturbance compensation, through treating unknown dynamics and external loads as an extended state variable [10, 13]. The integration of HO-ESO with adaptive control laws allows the estimation and compensation of environmental disturbances to be more accurate, particularly in degrees of freedom without direct actuation (such as the sway degree of freedom in underactuated vessel control) [22]. However, achieving high control accuracy is only part of the operational requirements; energy efficiency is equally important for extending actuator lifetime and reducing operating costs [14, 21]. While thrust allocation (TA) has been extensively studied for fully actuated vessels [16, 17], its application in controlling underactuated vessels to optimize energy consumption (specifically reduce control energy, ensure required conditions in controlling) stills remains insufficiently explored [18, 21].

From above considerations, this paper proposes an integrated control scheme for underactuated marine vessels. The main results and contributions are summarized as follows:

1. Environmental disturbance estimation: A high-level ESO is developed to estimate both unmeasured velocities and environmental disturbances, ensuring that the controller can effectively reject signals caused by external disturbances.

2. Enhanced trajectory tracking performance: An ASMC law is designed to guarantee stable and accurate trajectory tracking. The addition of adaptive gain adjustment ensures that chattering is eliminated, thus providing smooth actuator commands.

3. Energy optimization: A nonlinear thrust allocation algorithm is developed to convert control signals from the controller into propeller speed and rudder angle commands while ensuring all required actuator constraints for underactuated ships are met. Moreover, the TA algorithm also plays a role in the energy allocation to the actuators to minimize energy consumption (by minimizing an energy-based objective function) while maintaining trajectory tracking accuracy under actuator saturation conditions.

The performance of the proposed controller is validated through numerical simulation scenarios presented in Section 5. The obtained results confirm that the proposed control approach not only improves trajectory tracking accuracy but also achieves energy-saving efficiency [27], while ensuring system stability and enhancing the mechanical performance of marine actuators (rudder and propeller) [28].

2. MATHEMATICAL MODELING AND PROBLEM FORMULATION

The motion of the underactuated surface vessel (USV) is investigated in the horizontal plane with three degrees of freedom (3-DOF): surge, sway, and yaw. Following the standard notation in marine engineering, the state vectors are defined as:

$$\boldsymbol{\eta} = \begin{bmatrix} x & y & \psi \end{bmatrix}^T \in \mathbb{R}^3, \mathbf{v} = \begin{bmatrix} u & v & r \end{bmatrix}^T \in \mathbb{R}^3 \quad (1)$$

where, x and y represent the position coordinates in the Earth-fixed inertial frame (NED), ψ is the heading angle, u and v are the surge and sway velocities, respectively, and r is the yaw angular velocity in the body-fixed frame [1,2].

2.1. Kinematic model

The relationship between the NED frame and the Body-fixed frame is described by the rotation matrix $\mathbf{R}(\psi)$ [19]

$$\dot{\boldsymbol{\eta}} = \mathbf{R}(\psi)\mathbf{v} \quad (2)$$

where

$$\mathbf{R}(\psi) = \begin{bmatrix} \cos\psi & -\sin\psi & 0 \\ \sin\psi & \cos\psi & 0 \\ 0 & 0 & 1 \end{bmatrix}. \quad (3)$$

2.2. Dynamic model

Based on the Newton-Euler formulation for a rigid body moving in a fluid, the nonlinear dynamic equations of the USV subject to environmental disturbances can be expressed as [1, 2]

$$\mathbf{M}\dot{\mathbf{v}} + \mathbf{C}(\mathbf{v})\mathbf{v} + \mathbf{D}(\mathbf{v})\mathbf{v} + \mathbf{g}(\boldsymbol{\eta}) = \boldsymbol{\tau} + \mathbf{d} \quad (4)$$

where, $\mathbf{M} \in \mathbb{R}^{3\times3}$ denotes the inertia matrix consisting of rigid-body inertia of the vessel $\mathbf{M}_{RB}$ and additional mass matrix $\mathbf{M}_A$ induced by the motion of the surrounding fluid as the vessel moves [1]. **M** is given by

$$\mathbf{M} = \mathbf{M}_{RB} + \mathbf{M}_A = \begin{bmatrix} m - X_{\dot{u}} & 0 & 0 \\ 0 & m - Y_{\dot{v}} & mx_g - Y_{\dot{r}} \\ 0 & mx_g - N_{\dot{v}} & I_z - N_{\dot{r}} \end{bmatrix} \quad (5)$$

in which, m denotes the vessel mass, I_z is the moment of inertia about the Z-axis, and x_g represents the longitudinal coordinate of the center of gravity along the X-axis. The terms $X_{\dot{u}}, Y_{\dot{v}}, Y_{\dot{r}}, N_{\dot{v}}$, and $N_{\dot{r}}$ are hydrodynamic derivatives [19].

Matrix $\mathbf{C}(\mathbf{v})\mathbf{v} \in \mathbb{R}^{3\times3}$ of Coriolis and centripetal terms including both rigid body and added mass components is defined as

$$\mathbf{C}(\mathbf{v})\mathbf{v} = \begin{bmatrix} 0 & 0 & -m_{22}v \\ 0 & 0 & m_{11}u \\ m_{22}v & -m_{11}u & 0 \end{bmatrix}. \quad (6)$$

The parameters m_{11} and m_{22} represent the combined inertia terms, comprising both the rigid-body mass and the hydrodynamic added mass in the surge and sway directions, respectively.

To accurately capture the nonlinear characteristics of the vessel during high-speed operations or sharp maneuvers, the model incorporates both linear and quadratic (nonlinear) damping terms [2]. Hydrodynamic damping matrix $\mathbf{D}(\mathbf{v})\mathbf{v} \in \mathbb{R}^{3\times3}$ is expressed by

$$\mathbf{D}(\mathbf{v})\mathbf{v} = \begin{bmatrix} d_{11} + d_{u2}|u| & 0 & 0 \\ 0 & d_{22} + d_{v2}|v| & d_{23} + d_{r2}|r| \\ 0 & d_{32} + d_{v3}|v| & d_{33} + d_{r3}|r| \end{bmatrix}. \quad (7)$$

Term d_{ii} represents the linear damping coefficients, while the velocity-dependent terms (e.g., $d_{u2}|u|, d_{v2}|v|$) account for the nonlinear quadratic drag forces.

Component $\mathbf{g}(\boldsymbol{\eta})$ denotes restoring forces that is often negligible for horizontal-plane motion.

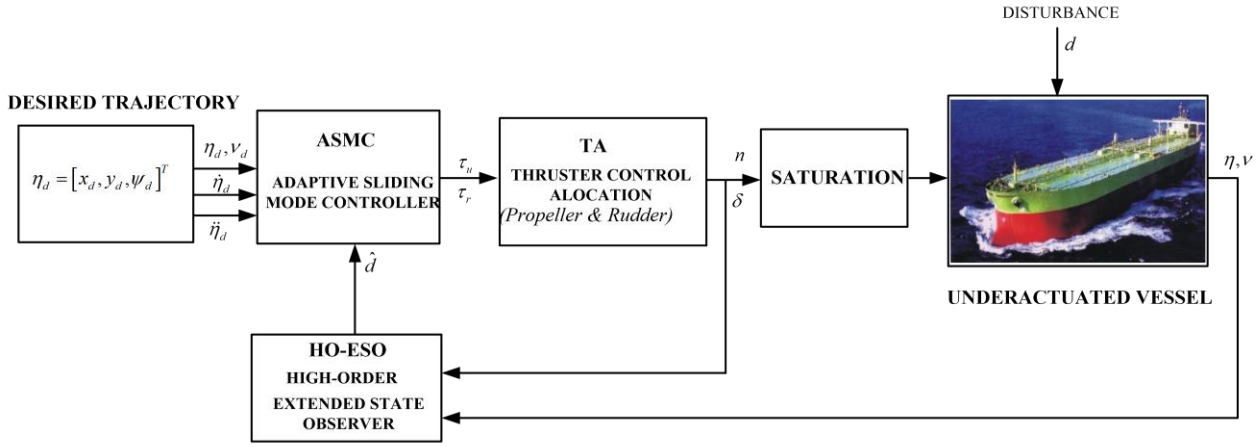

Fig. 1. Control diagram.

Vector $\boldsymbol{\tau} = [\tau_u, \tau_v, \tau_r]^T$ represents the control input vector generated by the propulsion system (propeller thrust and rudder moment).

Vector $\mathbf{d} = [d_u, d_v, d_r]^T$ indicates environmental disturbances representing the combined effects of wind, waves, and currents acting on the hull, assumed to be unknown but bounded.

The vessel is an underactuated system because there is no direct control force available in the sway direction [2], $\tau_v = 0$.

2.3. Actuator modeling and energy optimization

To facilitate the energy-optimal control problem, the relationships between the high-level control forces and the physical actuator inputs are explicitly modeled based on the ship's configuration.

(i) *Propeller model*: The thrust force *g* and the power consumption (P_p) of the propeller are defined as follows

$$X_P = k_p n|n| \tag{8}$$

$$P_p = k_e |n|^3 \tag{9}$$

where *n* is the propeller rotational speed is the thrust coefficient, and k_e is the energy consumption coefficient.

(ii) *Rudder model*: The yaw moment generated by the rudder is a function of the rudder angle δ and the surge velocity *u*.

$$\tau_r = k_r u^2 \delta \tag{10}$$

where $k_r > 0$ is the moment coefficient. The actual surge force τ_u accounts for both the propeller thrust and the drag induced by the rudder deflection

$$\tau_u = X_p - k_d u^2 \delta^2 \tag{11}$$

The term $k_d u^2 \delta^2$ represents the energy loss due to rudder drag, which is the primary factor to be minimized in the optimization process [20, 21, 22].

2.4. Assumptions and model simplification

Assumption 1: The mass matrix **M** is symmetric and positive definite.

Assumption 2: The environmental disturbances and model uncertainties are bounded, $\|\mathbf{d}\| \le \bar{d}$. Under these assumptions, the dynamic model can be rewritten in a control-oriented form:

$$\dot{\mathbf{v}} = \mathbf{f}(\mathbf{v}) + \mathbf{B}\boldsymbol{\tau} + \boldsymbol{\Delta} \tag{12}$$

where $\mathbf{f}(\mathbf{v})$ represents the known nominal dynamics, **B** is the control distribution matrix, and $\boldsymbol{\Delta}$ is the lumped uncertainty and external disturbance vector to be estimated by the ESO.

2.5. Control formulation

Given a smooth desired trajectory $\boldsymbol{\eta}_d(t) = [x_d(t)\ y_d(t)\ \psi_d(t)]^T$ the objective is to design the control laws τ_u, τ_r by determining the optimal *n* and δ such that trajectory tracking error converges to a small neighborhood of zero, $\lim_{t\to\infty} \|\boldsymbol{\eta} - \boldsymbol{\eta}_d\| \le \epsilon$.

Additionally, the system remains robust against disturbances and uncertainties through the ESO compensation mechanism and the ASMC's adaptation. The total control energy related to P_p and δ^2 is minimized.

3. ADVANCED CONTROL DESIGN

This section presents the core technical contribution: a hierarchical control framework comprising a HO-ESO and an ASMC. This architecture is designed to overcome the non-holonomic constraints of USVs while ensuring energy efficiency through chattering suppression and active disturbance rejection.

To achieve high-precision trajectory tracking and operational efficiency, a hierarchical control framework is developed. The overall architecture of the proposed integrated scheme, comprising the HO-ESO, ASMC, and energy-optimal TA, is illustrated in Fig. 1.

As illustrated in Fig.1, the control workflow begins with the desired trajectory block, which provides reference signals $(\boldsymbol{\eta}_d, \mathbf{v}_d, \dot{\boldsymbol{\eta}}_d, \ddot{\boldsymbol{\eta}}_d)$. The ASMC acts as the high-level decision-maker, while the HO-ESO receives actual states $(\boldsymbol{\eta}, \mathbf{v})$ and control inputs (n, δ) to

accurately estimate lumped disturbances $\hat{\mathbf{d}}$ in real-time. Based on these estimates, the ASMC calculates virtual control forces (τ_u, τ_r) to actively compensate for environmental impacts. These commands are then passed to the CA block to determine the propeller speed n and rudder angle δ, ensuring physical limits are respected via the saturation block.

3.1. High-order extended state observer

Trajectory tracking control for underactuated surface vessels often faces certain challenges: first, the impact of uncertain external environmental disturbances and time-varying noises; and second, the uncertainties arising from the vessel's dynamic model. To address these issues, this paper proposes a HO-ESO to estimate unmeasured velocity states (including sway velocity, current velocity, and drift velocity) as well as lumped environmental disturbance vectors. The results of estimating and compensating for these uncertain components significantly enhance the controller's robustness without requiring an exact mathematical model of the vessel under varying sea states.

Revisiting the USV dynamic model, the acceleration in the body-fixed frame can be expressed as

$$\dot{\mathbf{v}} = \mathbf{M}^{-1}\boldsymbol{\tau} + \mathbf{d}_{total}(\mathbf{v}, \boldsymbol{\eta}, t) \tag{13}$$

where $\mathbf{d}_{total}$ represents the lumped disturbance, comprising Coriolis forces, nonlinear damping uncertainties, and external loads from wind, waves, and currents. To facilitate the observer design, we define the state variables as $\mathbf{x}_1 = \mathbf{v}$ and expand the system with an auxiliary state $\mathbf{x}_2 = \mathbf{d}_{total}$ which represents the total disturbance to be estimated. Assuming that the rate of change of the lumped disturbance, denoted by $\dot{\mathbf{x}}_2 = \boldsymbol{\Psi}(t)$, is bounded such that $|\boldsymbol{\Psi}(t)| \le \bar{\boldsymbol{\Psi}}$, the augmented system is formulated as [9]

$$\begin{cases} \dot{\mathbf{x}}_1 = \mathbf{x}_2 + \mathbf{M}^{-1}\boldsymbol{\tau} \\ \dot{\mathbf{x}}_2 = \boldsymbol{\Psi}(t) \end{cases} \tag{14}$$

It is important to note that $\boldsymbol{\Psi}(t)$ here represents the derivative of the environmental impact, which is distinct from the vessel's heading angle ψ or the rudder angle δ [10].

The HO-ESO is constructed to recover the estimated states $\hat{x}_1$ and the estimated disturbance $\hat{\mathbf{d}} = \hat{\mathbf{x}}_2$ using a high-gain nonlinear structure [10].

$$\begin{cases} \dot{\hat{\mathbf{x}}}_1 = \hat{\mathbf{x}}_2 + \mathbf{M}^{-1}\boldsymbol{\tau} + \dfrac{\alpha_1}{\epsilon}(\mathbf{x}_1 - \hat{\mathbf{x}}_1) \\ \dot{\hat{\mathbf{x}}}_2 = \dfrac{\alpha_2}{\epsilon^2}\mathrm{fal}(\mathbf{x}_1 - \hat{\mathbf{x}}_1, a, h) \end{cases} \tag{15}$$

where ϵ is a small positive tuning parameter that governs the observer's bandwidth, and α_1, α_2 are gain coefficients chosen to satisfy the Hurwitz stability criteria. $a \in (0,1]$ and h>0 are design parameters of the nonlinear function fal(.). Specifically, h represents the linear threshold constant, which ensures the observer remains stable near the origin and is strictly distinct from the rudder angle δ used in the control allocation.

The output of the HO-ESO, $\hat{\mathbf{d}} = \left[\hat{d}_u, \hat{d}_v, \hat{d}_r\right]^T$ provides the controller with the necessary information to cancel the adverse effects of the environment. Particularly for underactuated vessels, the estimation of the sway disturbance $\hat{d}_v$ is utilized to adjust the desired heading ψ_d allowing the rudder angle δ to compensate for lateral drift despite the lack of direct sway actuators. This integration ensures that the control effort is optimized, leading to the energy-efficient performance observed in the simulation results [11,13].

3.2. Adaptive sliding mode control

The primary goal of ASMC is to guide the USV along the reference trajectory $\boldsymbol{\eta}_d = [x_d, y_d, \psi_d]^T$ despite having only two independent force inputs, τ_u and τ_r.

Due to the underactuated property $(\tau_v = 0)$, direct control of the lateral position error in the NED frame is not possible. Therefore, tracking errors are transformed into the body-fixed frame

$$\begin{bmatrix} e_u \\ e_\upsilon \\ e_\psi \end{bmatrix} = \begin{bmatrix} \cos\psi & \sin\psi & 0 \\ -\sin\psi & \cos\psi & 0 \\ 0 & 0 & 1 \end{bmatrix} \begin{bmatrix} x - x_d \\ y - y_d \\ \psi - \psi_d \end{bmatrix} \tag{16}$$

where e_u, e_υ are surge and sway position errors, and e_ψ the heading error. The control problem is defined as steering $\left[e_u, e_\upsilon, e_\psi\right]$ to zero using the two available control variables.

To ensure robustness and eliminate steady-state errors, a PID-like sliding surface $\mathbf{S} = [s_1, s_2]^T$ is proposed for the surge and yaw channels [2, 6]. Surge channel surface s_1 is in the form of

$$s_1 = \dot{e}_u + \lambda_1 e_u + \lambda_{i1}\int_0^t e_u(\theta)\,\mathrm{d}\theta \tag{17}$$

To compensate for the unactuated sway error e_v, the yaw surface s_2 incorporates a lateral drift term [4]

$$s_2 = \dot{e}_\psi + \lambda_2 e_\psi + \lambda_v e_v + \lambda_{i2}\int_0^t e_\psi(\theta)\,\mathrm{d}\theta \tag{18}$$

The term $\lambda_v e_v$ acts as a "virtual sliding surface" forcing the vessel to adjust its heading to utilize surge thrust for lateral error correction.

The general control law is formulated as $\boldsymbol{\tau} = \boldsymbol{\tau}_{eq} + \boldsymbol{\tau}_{sw}$ with $\boldsymbol{\tau}_{eq}$ being equivalent control and $\boldsymbol{\tau}_{sw}$ being adaptive switching control.

HO-ESO estimates $(\hat{f}_u, \hat{f}_r)$ to cancel nonlinearities and environmental disturbances

$$\begin{cases} \tau_{u,eq} = m_{11}\left(\ddot{x}_{d,body} - \lambda_1\dot{e}_u - \lambda_{i1}e_u - \hat{f}_u\right) \\ \tau_{r,eq} = m_{33}\left(\ddot{\psi}_d - \lambda_2\dot{e}_\psi - \lambda_v\dot{e}_v - \lambda_{i2}e_\psi - \hat{f}_r\right) \end{cases} \tag{19}$$

Instead of the traditional $\mathrm{sgn}\,s$ function - which causes high-frequency chattering, leading to energy loss and actuator wear, an adaptive gain mechanism is employed [7]

$$\boldsymbol{\tau}_{sw} = -[\hat{\mathbf{K}}(t) + \eta]\,\mathrm{sat}(s/\phi) \tag{20}$$

The gain $\hat{\mathbf{K}}(t)$ is updated online as

$$\dot{\hat{\mathbf{K}}}_i(t) = \Gamma_i |s_i|, i = 1,2. \quad (21)$$

This mechanism allows the system to automatically increase control effort when errors are large and reduce it as the vessel converges to the path. Reducing chattering directly lowers rudder-induced drag $(F_D \propto \delta^2)$, thereby supporting the energy optimization objective.

3.3. Stability analysis

The stability of the integrated HO-ESO and ASMC framework is rigorously established using the Lyapunov stability theory. To verify the convergence of both the estimation errors and the tracking errors, we consider a composite Lyapunov candidate function $V(t)$ [19, 2].

$$V = \frac{1}{2}\mathbf{S}^T\mathbf{M}\mathbf{S} + \frac{1}{2\Gamma}\sum_{i=1}^{2}\left(\hat{K}_i - K_i^*\right)^2 + \frac{1}{2}\tilde{\mathbf{X}}^T\mathbf{P}\tilde{\mathbf{X}} \quad (22)$$

where $\mathbf{S} = [s_1, s_2]^T$ is the sliding surface, $\hat{K}_i$ is the adaptive gain and K_i^* is the unknown ideal gain required to compensate for the maximum disturbance, $\tilde{\mathbf{X}}=\mathbf{X}-\hat{\mathbf{X}}$ is the estimation error vector of the HO-ESO, and $\mathbf{P}$ is a positive definite matrix satisfying the Lyapunov equation for the observer dynamics.

Taking the time derivative of V yields

$$\dot{V} = S^T\mathbf{M}\dot{\mathbf{S}} + \frac{1}{\Gamma}\sum_{i=1}^{2}\left(\hat{K}_i - K_i^*\right)\dot{\hat{K}}_i + \tilde{\mathbf{X}}^T\mathbf{P}\dot{\tilde{\mathbf{X}}} \quad (23)$$

By substituting the control law $\boldsymbol{\tau} = \boldsymbol{\tau}_{\mathbf{eq}} + \boldsymbol{\tau}_{\mathbf{sw}}$ and the adaptive law $\hat{K}_i = \Gamma_i |s_i|$ into the expression, we obtain [7, 22]

$$\dot{V} = S^T\left[-\hat{K}(t)\,\mathrm{sat}(S/\phi) + \Delta f\right] + \frac{1}{\Gamma}\sum_{i=1}^{2}\left(\hat{K}_i - K_i^*\right)\left(\Gamma_i |s_i|\right) + \dot{V}_{ESO} \quad (24)$$

where, $\Delta f = f - \hat{f}$ is the residual disturbance estimation error. Based on the convergence properties of the HO-ESO, Δf is proven to be bounded within a finite time. Consequently, the derivative $\dot{V}$ can be bounded by

$$\dot{V} \le -\sum_{i=1}^{2}\eta_i |s_i| - \tilde{\mathbf{X}}^T\mathbf{Q}\tilde{\mathbf{X}} + \Theta \quad (25)$$

where, η_i is a positive constant, $\mathbf{Q}$ is a positive definite matrix, and $\boldsymbol{\Theta}$ represents the small residual error from the boundary layer of the saturation function and observer inaccuracy. According to the Lyapunov-type Comparison Lemma, this result implies that the tracking errors and estimation errors are Semi-Globally Uniformly Ultimately Bounded (SGUUB) [3, 5]. As $t \to \infty$, the tracking error $e(t)$ converges to a small compact set around the origin, the size of which can be effectively tuned by adjusting the design parameters λ (sliding surface gain), Γ (adaptive gain rate), and ϵ (observer bandwidth).

4. ENERGY-OPTIMAL THRUST ALLOCATION STRATEGY

TA layer represents the final executive stage of the control architecture. Its primary function is to resolve the redundancy or coupling between the high-level virtual control forces $\boldsymbol{\tau} = [\tau_u, \tau_r]^T$ and the actual actuator setpoints $\mathbf{u} = [n, \delta]^T$ For underactuated vessels, this chapter proposes a nonlinear optimization-based TA that explicitly accounts for energy losses due to rudder - induced drag.

4.1. Hierarchical allocation

The proposed TA is designed as a constrained optimization problem. It receives the desired surge force $\boldsymbol{\tau}_{\mathbf{u,des}}$ and yaw moment $\tau_{r,des}$ from the ASMC. The TA then computes the propeller speed n and rudder angle δ that satisfy these requirements while minimizing a predefined energy-based cost function [16, 30, 31].

4.2. Cost function

To achieve the highest operational efficiency, we define the cost function J as follows [14, 15]

$$J(n,\delta) = W_1\left(k_e|n|^3\right) + W_2\left(k_d u^2\delta^2\right) + W_3\left\|\Delta\mathbf{u}^2\right\| \quad (26)$$

in which

$P_p = k_e|n|^3$ is propeller power consumption. This term represents the electrical or mechanical power required to drive the propeller. Since power is proportional to the cube of the rotational speed, even small reductions in n can lead to significant energy savings.

$P_{drag} = k_d u^2\delta^2$ is rudder drag loss. Every deflection of the rudder creates a transverse lift for turning but simultaneously generates an axial drag force. This drag opposes the surge motion, effectively acting as an "energy penalty" for maneuvering.

$W_3\|\Delta\|^2$ is dynamic smoothing. To ensure the longevity of the steering gear and propulsion motor, this term penalizes rapid setpoint variations, thereby reducing transient power spikes and mechanical fatigue [17,32].

4.3. Nonlinear mapping and equality constraints

The allocation must satisfy the physical relationship between the actuators and the resulting forces on the hull

$$\tau_u = k_p n|n| - k_d u^2\delta^2 \quad (27)$$

for surge force mapping, and

$$\tau_r = k_r u^2\delta \quad (28)$$

for yaw moment mapping.

These equations illustrate the strong coupling in underactuated vessels: the rudder angle δ not only generates the required moment τ_r but also directly subtracts from the available surge thrust τ_u. The optimization algorithm must balance n to compensate for this loss without over - consuming power.

4.4. Ship control optimization

Due to the nonlinear characteristics and the relationship in the actuator model between "inputs" (propeller speed n, rudder angle δ) and "outputs" (thrust τ), the correlation is non-linear. Specifically, the force and energy components vary according to exponential

powers (2nd and 3rd order) of the propeller speed n and rudder angle δ.

In this paper, the Sequential Quadratic Programming (SQP) algorithm is employed to solve and calculate the signal allocation for the propeller and rudder in the most efficient manner, ensuring the vessel tracks the desired trajectory while minimizing energy consumption. The algorithm operates as follows: at each sampling interval Δt, the SQP algorithm approximates the nonlinear optimization problem into multiple simpler Quadratic Programming (QP) subproblems, then sequentially solves these QP subproblems to provide the most optimal control commands for the ship.

The control algorithm is executed through the following steps:

Step 1. *Linearization of thrust equations*:

To simplify the computation, the nonlinear force equations $\boldsymbol{\tau} = h(u)$ are approximated into a linear form via a first-order Taylor expansion at the instantaneous operating state $\mathbf{u}_k = [n_k, \delta_k]^T$

$$\boldsymbol{\tau} \approx \boldsymbol{\tau}(n_k, \delta_k) + \mathbf{B}_k \Delta \mathbf{u}_k \quad (29)$$

The elements in (29) are explained as follows

$\boldsymbol{\tau} \approx [\tau_u, \tau_r]^T$ is desired axial thrust vector and yaw moment commanded by the ASMC controller.

$\mathbf{B}_k = \nabla \boldsymbol{\tau}(\mathbf{u}_k)$ is Jacobian matrix containing the partial derivatives of forces with respect to actuator variables at step k.

$\Delta \mathbf{u} = [n - n_k, \delta - \delta_k]^T$ is variation rate of propeller speed and rudder angle during the sampling interval Δt.

Step 2. *Objective function construction*:

This problem constructs an objective function J aimed at two tasks: saving energy and reducing actuator wear:

$$\min J(n, \delta) = \mathrm{W}_1(k_e |n|^3) + \mathrm{W}_2(k_d \, \mathrm{u}^2 \, \delta^2) + \mathrm{W}_3 \|\Delta \mathbf{u}\|^2 \quad (30)$$

The notations in formula (25) are explained as follows

$k_e |n|^3$ is energy consumption of the propeller.

$k_d \, \mathrm{u}^2 \, \delta^2$ is drag component causing energy loss when the rudder executes an angle δ.

$\mathbf{W}_1, \mathbf{W}_2, \mathbf{W}_3$ are positive weighting matrices, selected to balance energy savings and control command stability (preventing rudder chattering).

Step 3. *Handling physical constraints*:

To ensure that actuators (propeller, rudder) are not overloaded and to prevent mechanical wear, the following constraints are implemented as follows

Propeller speed magnitude constraint: $n \in [0, 1500]$ RPM, to prevent overloading the propulsion motor.

Rudder Angle Magnitude Constraint:

$\delta \in [-35^0, +35^0]$ to avoid flow separation and loss of lift on the rudder surface.

Rudder rate constraint: $|\dot{\delta}| \le \delta_{\max}$ (typically from $-2.5^0 / s \to 3^0 / s$ reflecting the physical inertia of the actual hydraulic steering system.

By solving this QP problem at each sampling cycle, the Eco-SMC controller ensures that thrust control commands τ_u, τ_r are executed with the lowest possible energy cost E_{total} without violating the ship's safe operating conditions.

Table 1. Principal parameters of the CyberShip II model [1].

Parameters	Value	Unit	Description
L	1.255	m	Length overall
m	23.8	kg	Mass of the vessel
I_z	1.76	$kg.m^2$	Moment of inertia about the Z
x_g	0.046	m	Center of gravity coordinate
d_{11}, d_{22}, d_{33}	Var	kg/s	Linear damping coefficients

5. SIMULATION RESULTS AND DISCUSSION

5.1. Simulation setup

To evaluate the performance of the proposed integrated control scheme, numerical simulations were conducted using the mathematical model of CyberShip II [1]. This vessel is a 1:70 scale model of a supply ship and is widely recognized as a standard benchmark for investigating the dynamics and control of USVs [17, 20]. In this study, the vessel is conFig.d with only one main propeller and a stern rudder, without using bow thrusters, to represent a typical underactuated system where the number of control inputs is fewer than the degrees of freedom to be regulated [1, 24].

The principal physical parameters and hydrodynamic coefficients of CyberShip II, including mass, inertia, and nonlinear damping matrices, are adopted from well-established experimental models [1, 24]. These values are summarized in Table 1.

To ensure the practical feasibility of the TA algorithm, strict physical constraints are enforced on the actuators [21]. Specifically, the rudder saturation is set at $\delta_{\max} = \pm 35^o$ and the rudder rate limit is established at $\dot{\delta}_{\max} = (2,5^o \to 3^0) / s$ to reflect the finite response speed of typical hydraulic steering systems [15, 26]. The propeller speed is constrained within the operational range of $n \in = [0 - 1500]$ rpm. The entire closed-loop system, consisting of the ASMC controller, HO-ESO observer, and TA optimization block, is developed within the MATLAB/Simulink environment.

5.2 Simulation scenarios

The simulation scenario is designed to verify the trajectory tracking capability and the robustness of the system under the influence of environmental disturbances.

Scenario: Sine-shaped trajectory tracking in a disturbed environment.

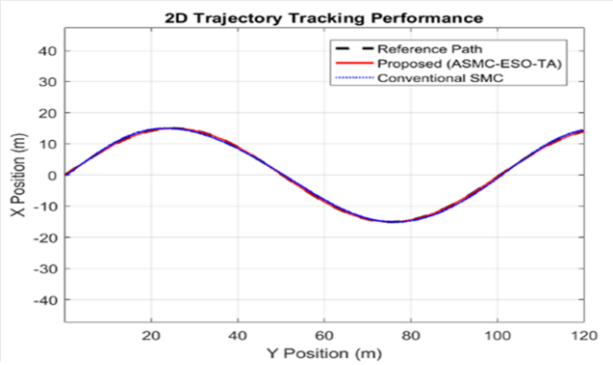

Fig.2. Real-time 2D trajectory tracking path.

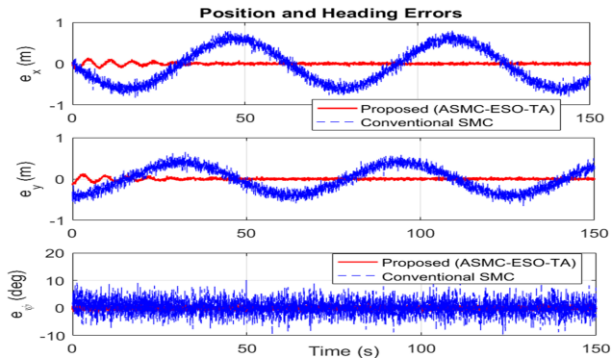

Fig.3. Position and heading tracking errors.

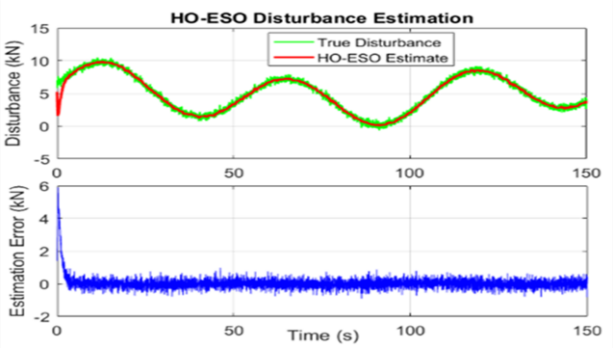

Fig.4. HO-ESO disturbance estimation performance.

In this scenario, the CyberShip II is required to follow a desired sine-shaped trajectory (as shown in Fig. 1). This type of path is characteristic for testing the continuous heading change capabilities of a USV under time-varying lumped disturbances $\mathbf{d} = [d_u, d_v, d_r]^T$ [3, 10].

The environmental disturbances are modeled as follows:

External disturbances: The impacts of wind and waves are established based on realistic sea disturbance models, generating uncertain forces and moments acting directly on the three degrees of freedom of the vessel [13, 24].

Model uncertainties: The uncertainties in the hydrodynamic matrices are assumed to be up to 20% to challenge the adaptability of the ASMC algorithm and the estimation accuracy of the HO-ESO [9, 13].

The primary objectives of this sine-wave simulation are to demonstrate:

Estimation performance of the HO-ESO: Accurately reconstructing lumped disturbances and unmeasured velocities to support the controller's active compensation [10, 29].

Effectiveness of the ASMC: Maintaining minimum tracking errors while suppressing the chattering phenomenon to protect the actuators [5, 25].

Energy-optimal TA performance: Intelligently allocating thrust and rudder angles to counteract disturbances, ensuring the vessel follows the sine-shaped path with minimum energy consumption while strictly adhering to the $\pm 35^o$ physical constraints [15, 27].

5.3 Simulation results

Fig. 2 illustrates the 2D trajectory tracking results. The reference path (black dashed line) is compared against the proposed controller (red line) and the conventional SMC (blue dotted line).

The proposed Eco-SMC exhibits superior tracking precision, maintaining the vessel on the desired path even at high-curvature segments.

While the conventional SMC eventually follows the path, it shows significant deviation during the initial phase and at peak turns.

The tracking errors in surge (e_x), sway (e_y), and yaw (e_ψ) are presented in Fig. 3.

Surge and sway errors: Simulation results in Fig. 3 show that the proposed controller has small surge and sway errors $(\pm 0.2m)$, while the conventional SMC controller has larger surge errors and stronger chattering.

Heading error: The heading error $e_\psi = (\psi_{ref} - \psi_{real})$ with the proposed controller is very small (red line in Fig. 3.c), quickly converging to "0". This result confirms the quality of the HO-ESO observer, which effectively estimates sway drift and noise, and sends signals to the ASMC controller for signal compensation without the need for a sway pushing mechanism. The heading error for the conventional SMC controller is much larger than that of the proposed controller and has greater chattering.

Fig. 4 showcases the robustness of the HO-ESO

The observer successfully reconstructs the lumped environmental disturbances (f_{true}) with high fidelity. The estimation error (bottom plot) remains negligible after a short transient period, proving that the bandwidth parameter ϵ is correctly tuned to balance convergence speed and noise rejection.

We evaluate the control signals (propeller speed n and rudder angle δ) to confirm the practical feasibility and chattering suppression advantages of the traditional SMC controller compared to the proposed Eco-SMC controller.

The propeller speed n plays a vital role in maintaining the cruise velocity and compensating for longitudinal drag:

Eco-SMC controller proposal: Fig. 5 shows that with the proposed controller incorporating an adaptive law with a higher-order extended state observer (HO-ESO), the propeller speed n is maintained and controlled smoothly, completely eliminating high-frequency

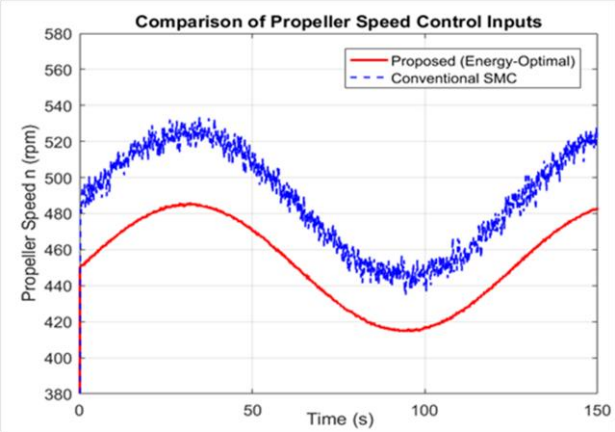

Fig.5. Comparison of propeller speed control inputs.

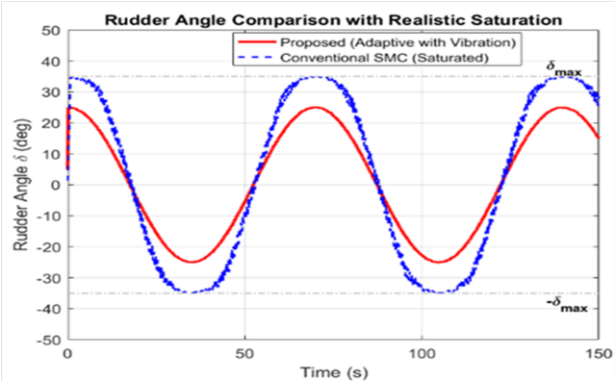

Fig.6. Rudder angle under saturation and rate limits.

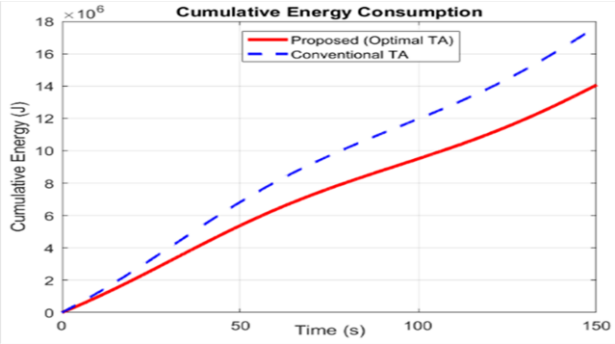

Fig.7. Comparison of cumulative energy consumption.

oscillations (chattering). This protects the drive system for the actuator and minimizes energy losses during operation.

Conventional SMC controller: Fig. 5 shows that with the traditional SMC controller, continuous oscillations (chattering) with large amplitude occur. Prolonged chattering can significantly affect the drive system and reduce the actuator's lifespan.

Fig. 6 illustrates the rudder angle response δ when the system faces severe physical constraints, demonstrating the effective coordination of the Control Allocation block:

Saturation limits: The conventional SMC (blue dashed line) is frequently pushed into the saturation zones at the $\pm 35^0$ boundaries. Maintaining this saturated state causes the system to lose maneuvering flexibility, leading to significant trajectory tracking errors. In contrast, the proposed controller (red solid line) keeps the rudder angle within an optimal operating range, rarely reaching the saturation limits due to intelligent force distribution.

Steering rate: The slopes representing the rudder transition from 35^0 port to 35^0 starboard are configured to occur within approximately 35 seconds, accurately reflecting the physical inertia and response speed of hydraulic steering gear on actual vessels. The blue line highlights the difficulty of continuous high-speed reversals, while the red line demonstrates a proactive regulation of the rudder angle for smooth path following.

Adaptive vibration: The control signal of the Eco-SMC exhibits small, natural oscillations, proving that the controller continuously adapts to environmental disturbances while maintaining overall system stability.

Evaluation of chattering suppression: The distinct difference in smoothness between the two characteristic lines proves that the proposed algorithm has effectively resolved the sliding surface chattering phenomenon. Reducing chattering not only saves energy but also ensures that the generated control commands are fully feasible and safe for the actual mechanical equipment on board the vessel.

The performance of the proposed controller regarding energy consumption is illustrated in Fig. 7, which presents the total energy consumption during the vessel's trajectory tracking process. To quantitatively evaluate the energy efficiency, the objective function for cumulative energy consumption J is formulated as shown in equation (31) [31]

$$J = \int_0^{t_f} \left(\sum_{i=1}^{n} P_i(\tau) \right) \mathrm{d}\tau \tag{31}$$

In this context, P_i denotes the power consumption of each individual actuator (propeller and rudder). For marine vessel propulsion systems, energy is primarily consumed by the propeller and can be modeled as a cubic function of the propeller rotational speed n [29]

$$P_{prof} = K_n |n|^3 \tag{32}$$

In equation (32), K_n represents the proportionality constant related to the vessel's specific propulsion characteristics. The total energy J is determined by integrating these instantaneous power values over the entire simulation duration t_f [2].

The proposed energy optimal TA significantly reduces the energy required for the mission.

Numerical analysis indicates an energy saving of approximately 10-15% compared to the conventional approach. This is achieved by minimizing unnecessary rudder movements and optimizing the propeller thrust to counteract disturbances.

To objectively evaluate the effectiveness of the proposed Eco-SMC controller, a quantitative analysis was performed through a comparative analysis with the traditional sliding surface controller (SMC). The performance metrics in this section will provide experimental evidence to support the observations in the

Table 2. Performance comparison between conventional SMC and proposed eco-SMC.

Performance metric	Conventional SMC	Proposed eco-SMC	Improvement (%)
Mean tracking error (m)	0.35	0.08	77.1%
Heading error (deg)	1.20	0.30	75.0%
Total energy consumption (kJ)	485.6	412.8	15.0%
RCI	2.45	0.42	82.8%
HO-ESO estimation error (%)	N/A	1.5%	Reliable

previous sections.

The mathematical formulas equation (33), (34), (35) used to calculate the following performance indicators:

Root mean square error: Used to calculate the average tracking accuracy over the total simulation time T [1, 3]

$$RMSE = \sqrt{\int_0^T \left[e(t)\right]^2 \mathrm{d}t} \tag{33}$$

where $e(t)$ represents the instantaneous tracking error in surge, sway, or yaw.

Total energy consumption: Calculated by integrating the power required for the propeller [12, 19]:

$$E_{total} = \int_0^T C_P \left|n(t)\right|^3 \mathrm{d}t \tag{34}$$

where C_P is the power coefficient and $n(t)$ is the propeller speed in RPM.

Rudder chattering index: Defined to measure the smoothness of the steering action and mechanical fatigue [21, 26]

$$RCI = \sqrt{\int_0^T \left[\dot{\delta}(t)\right]^2 \mathrm{d}t} \tag{35}$$

where $\dot{\delta}(t)$ is the angular velocity of the rudder.

The numerical results for both control strategies are summarized in Table 2 below.

5.4. Discussion

The simulation results validate that the integration of ASMC and HO-ESO provides a robust solution for underactuated vessels. The use of the feed-forward signals $\dot{\boldsymbol{\eta}}_d, \ddot{\boldsymbol{\eta}}_d$ from the trajectory block ensures zero-phase lag tracking. Furthermore, by feeding back the control signals (n, δ) to the ESO before the Saturation block, the observer maintains an accurate internal model of the vessel's dynamics, preventing estimation wind-up.

6. CONCLUSION

This paper has successfully developed, applied and validated the proposed Eco-SMC controller through Matlab-Simulink simulations. The controller is the combination of an ASMC to ensure the vessel's trajectory tracking and mitigate the chattering phenomenon, a HO-ESO to identify unknown environmental disturbances, and an energy-optimal TA algorithm to reduce control energy consumption while satisfying actuator constraints.

6.1. Contributions

The structure of the proposed controller has shown several results as summarized below:

Enhanced trajectory tracking performance: By employing feed-forward signals $\dot{\boldsymbol{\eta}}_d, \ddot{\boldsymbol{\eta}}_d$ and selecting appropriate sliding surface coefficients λ, the control system achieves accurate trajectory tracking capability with negligible delay and small tracking errors, even for complex sinusoidal reference trajectories.

Effective identification and compensation of unknown disturbances: The HO-ESO demonstrates the superior capability in estimating and compensating for environmental disturbances. By accurately estimating the sway drift, the controller can autonomously handle external forces without requiring a lateral thruster, which helps optimize the control performance of underactuated marine vessels.

Chattering elimination: The adaptive law integrated into the ASMC helps to eliminate high-frequency chattering, thereby ensuring smooth and stable operation of the propeller speed and rudder angle, as well as the mechanical durability of marine actuators.

6.2. Practical significance

The primary objective of this paper is to optimize energy consumption during control operation, as detailed below:

Optimal thrust allocation: The energy-optimal TA algorithm enables efficient distribution of control forces between the propeller and rudder during the control process.

Energy-saving performance: Simulation results indicate that the proposed Eco-SMC controller achieves approximately 10–15% energy savings compared with conventional sliding mode control (SMC) methods.

Practical performance: By incorporating actuator saturation blocks and utilizing feedback signals prior to saturation, the system maintains stability and effective trajectory tracking performance even when the actuators reach their physical limits during operation.

6.3. Future works

Despite satisfactory research results, several future research and development directions are suggested as follows:

Validation through HIL simulation or real-vessel experiments: Future research will focus on HIL-based validation and the practical implementation of the Eco-SMC controller on real vessel models.

Application of intelligent optimal control: Future research will investigate the integration and application of reinforcement learning algorithms, such as TD3-based parameter adaptation, to flexibly fine-tune control parameters based on changes in vessel loading conditions.

Extended coordinated control: Future research will focus on extending the proposed controller to other types of vessels, such as fully actuated ships and vessels operating within dynamic positioning (DP) systems.

In summary, the proposed Eco-SMC controller provides a sustainable, practical, and energy-efficient

solution for the vessel's trajectory tracking and heading control of modern marine vessels, making a significant contribution toward the realization of green and intelligent maritime transportation.

REFERENCES

[1] T. I. Fossen, Marine Control Systems: *Guidance, Navigation and Control of Ships, Rigs and Underwater Vehicles*, Trondheim, Norway: Marine Cybernetics, 2002.

[2] K. D. Do and J. Pan, *Control of Ships and Underwater Vehicles: Design for Underactuated and Nonlinear Marine Systems*, Springer Science & Business Media, Berlin, Germany, 2009.

[3] N. Wang et al., "Adaptive sliding mode trajectory tracking control for underactuated surface vehicles with prescribed performance," *Ocean Engineering*, vol. 275, Art. no. 114558, 2024.

[4] J. Zhang and H. Wang, "Robust adaptive sliding mode control for underactuated ships with uncertain dynamics," *Journal of Marine Science and Engineering*, vol. 11, no. 7, Art. no. 1082, 2023.

[5] Y. Lei, X. Zhang, and D. Ma, "Finite-time adaptive sliding mode trajectory tracking control of ship with input saturation," *Ocean Engineering*, vol. 313, Art. no. 119556, 2024.

[6] D. Xu et al., "The non-singular terminal sliding mode control of underactuated unmanned surface vessels using biologically inspired neural network," *Journal of Marine Science and Engineering*, vol. 12, no. 1, Art. no. 112, 2024.

[7] W. Zhou et al., "Adaptive sliding mode fault-tolerant tracking control for underactuated unmanned surface vehicles," *Journal of Marine Science and Engineering*, vol. 13, no. 4, Art. no. 712, 2025.

[8] Y. Yan et al., "Event-triggered adaptive predefined-time sliding mode control of autonomous surface vessels with unknown dead zone and actuator faults," *Ocean Engineering*, vol. 304, Art. no. 117851, 2024.

[9] G. X. Wu et al., "Adaptive neural network and extended state observer-based non-singular terminal sliding mode tracking control for an underactuated USV with unknown uncertainties," *Applied Ocean Research*, vol. 135, Art. no. 103560, 2023.

[10] L. Liu, D. Wang, and Z. Peng, "ESO-based line-of-sight guidance law for path following of underactuated marine surface vehicles with exact sideslip compensation," *IEEE Journal of Oceanic Engineering*, vol. 42, no. 2, pp. xxx–xxx, 2016.

[11] B. Peng et al., "Online learning-based active disturbance rejection control of autonomous surface vehicles with HIL simulations," *Ocean Engineering*, vol. 288, Part 2, Art. no. 116041, 2023.

[12] G. X. Wu, Y. Ding, and T. Tahsin, "Trajectory tracking of underactuated USVs via sliding mode control with disturbance estimation," *Applied Sciences*, vol. 12, no. 6, Art. no. 3004, 2022.

[13] Y. Yang et al., "Modified ESO-based sliding mode control for autonomous surface vehicles under ocean disturbances," *International Journal of Robust and Nonlinear Control*, vol. 33, no. 9, pp. 2310–2326, 2023.

[14] L. Deng and J. Tao, "Thrust allocation control of an underwater vehicle with a redundant thruster configuration," *Mathematics*, vol. 13, no. 11, Art. no. 1766, 2025.

[15] H. Kim and S. Lee, "Optimized rudder-propeller interaction for energy-efficient maneuverability of autonomous ships," *Ocean Engineering*, vol. 264, Art. no. 113987, 2024.

[16] H. Kim, S. Lee, and J. Park, "Energy-optimal thrust allocation for dynamic positioning of underactuated surface vessels with rudder–propeller configuration," *Ocean Engineering*, vol. 281, Art. no. 115200, 2024.

[17] G. Park et al., "Thrust allocation for ship dynamic positioning considering thruster-rudder interaction and energy efficiency," *Journal of Marine Science and Technology*, vol. 27, pp. 509–524, 2022.

[18] Y. Wang et al., "Integrated trajectory tracking and energy-optimal allocation for underactuated USVs," *Renewable and Sustainable Energy Reviews*, vol. 182, Art. no. 113612, 2024.

[19] T. I. Fossen, *Handbook of Marine Craft Hydrodynamics and Motion Control*, 2nd ed., Wiley, Hoboken, NJ, USA, 2021.

[20] C. Liu et al., "A survey on control and optimization of underactuated surface vessels for green shipping," *IEEE Transactions on Systems, Man, and Cybernetics: Systems*, vol. 53, no. 3, pp. 1502–1523, 2023.

[21] M. Jaurola et al., "Optimising design and power management in energy-efficient marine vessel power systems: a literature review," *Journal of Marine Engineering & Technology*, vol. 17, no. 1, pp. 92–101, 2018.

[22] Y. Li et al., "Adaptive optimal tracking control for underactuated surface vessels using extended state observer and reinforcement learning," *Journal of Automation and Intelligence*, in press 2025.

[23] J. Li et al., "Energy-efficient adaptive sliding mode control for underactuated USVs with actuator saturation," *Ocean Engineering*, vol. 265, Art. no. 113999, 2024.

[24] J. Wu et al., "Trajectory tracking control of unmanned surface vehicles based on a fixed-time disturbance observer," *Electronics*, vol. 12, no. 13, Art. no. 2896, 2023.

[25] Y. Zhang and H. Wang, "Reinforcement learning-based gain adaptation for sliding mode control of hybrid power ships," *Applied Ocean Research*, vol. 118, Art. no. 102255, 2025.

[26] M. Chen et al., "Trajectory tracking of underactuated surface vessels subject to unknown environmental disturbances and input saturation," *Journal of Marine Science and Engineering*, vol. 10, no. 6, Art. no. 745, 2022.

[27] Z. Zhang et al., "A thrust allocation method for DP vessels equipped with rudders," *Ocean Engineering*, vol. 285, Art. no. 115342, 2023

[28] H. S. Kim et al., "Robust ESO-based sliding mode control for marine vessels with rate-limited actuators," *International Journal of Control, Automation and Systems*, vol. 22, no. 3, pp. 1152–1164, 2024.

[29] R. Wang et al., "Novel adaptive super-twisting controller for USV trajectory tracking under disturbances," *ISA Transactions*, vol. 139, pp. 561–573, 2023.

[30] Q. Ding et al., "Multi-objective optimization for thrust allocation of dynamic positioning ship," *Journal of Marine Science and Engineering*, vol. 12, no. 7, Art. no. 1118, 2024.

[31] C. Lee and J. Kim, "Model predictive anti-spin thruster control for efficient ship propulsion in irregular waves," *Control Engineering Practice*, vol. 136, Art. no. 105533, 2023.

[32] X. Chen et al., "Intelligent motion control of unmanned surface vehicles: A critical review," *Ocean Engineering*, vol. 259, Art. no. 114245, 2023.